Chinese Journal of
POLYMER SCIENCE

RESEARCH ARTICLE

https://doi.org/10.1007/s10118-026-3744-0
Chinese J. Polym. Sci.

Microgels Deswell against Concentration and Solvent Molecular Mass

Yi-Hui Zhu[a,†], Qing-Zhi Zou[b,c,†], Zhan-Hui Gan[d], Yi-Fu Ruan[d], Kai Qi[b,c], Peng-Fei Zhang[a], and Geng-Xin Liu[a*]

[a] *State Key Laboratory of Advanced Fiber Materials, Center for Advanced Low-dimension Materials, College of Materials Science and Engineering, Donghua University, Shanghai 201620, China*
[b] *2020 X-Lab, Shanghai Institute of Microsystem and Information Technology, Chinese Academy of Sciences, Shanghai 200050, China*
[c] *Center of Materials Science and Optoelectronics Engineering, University of Chinese Academy of Sciences, Beijing 100049, China*
[d] *South China Advanced Institute for Soft Matter Science and Technology, School of Emergent Soft Matter & Guangdong Provincial Key Laboratory of Functional and Intelligent Hybrid Materials and Devices, South China University of Technology, Guangzhou 510640, China*

Electronic Supplementary Information

Abstract The deswelling of microgels is governed by solvent characteristics and particle concentration. Soft nanoparticles have been synthesized and dispersed in small molecular solvents or oligomeric polystyrenes. Coarse-grained molecular dynamics simulations were performed to quantify particle dimensions. The linear viscoelasticity of these solutions was experimentally characterized. In good solvents, increasing the particle concentration induces deswelling because of the enhanced crowding-induced osmotic compression. Increasing the molecular mass of the solvent could also enhance deswelling by suppressing solvent penetration into the nanoparticle network. Equilibrium relations derived from the osmotic-pressure balance are developed to describe these two mechanisms and are shown to capture the simulation results. A single unified framework can describe the deswelling over a broad range of solvent masses and particle concentrations. In addition, varying the solvent mass shifts the fragility transition observed experimentally in solutions of soft nanoparticles, thereby linking deswelling to changes in the glassy dynamics. This work establishes a unified framework for understanding microgel deswelling across concentration- and solvent-controlled regimes.

Keywords Deswelling; Microgel; Concentration dependence; Fragility; Equation of state

Citation: Zhu, Y. H.; Zou, Q. Z.; Gan, Z. H.; Ruan, Y. F.; Qi, K.; Zhang, P. F.; Liu, G. X. Microgels deswell against concentration and solvent molecular mass. *Chinese J. Polym. Sci.* https://doi.org/10.1007/s10118-026-3744-0

INTRODUCTION

Polymeric nanoparticles dispersed in molecular or oligomeric media can exhibit solvent interaction, leading to pronounced changes in their effective size and softness.[1–5] Such "swollen" polymeric colloids occupy an effective volume that differs substantially from their dry volume, thereby reshaping interparticle interactions, rheology, and glass transition.[6–10] Establishing physically transparent routes to control nanoparticle swelling and deswelling is therefore central to studying polymer–solvent nanocomposites and soft colloids dynamics.

Previous studies on polymeric soft colloids have focused predominantly on dilute dispersions of charged microgels and nanogels, in which swelling is governed by a balance among mixing thermodynamics, network elasticity, and electrostatic contributions, and is commonly tuned by temperature, pH, ionic strength, added salt, and solvent quality.[11–15] As a result, mechanistic understanding is most developed for charged systems in the dilute limit. In contrast, neutral polymer nanoparticles have been explored much less extensively, particularly in concentrated dispersions. Although increasing concentrations has shown to induce particle deswelling and to couple particle softness to crowding, vitrification, and fragility, available studies remain limited. [16–18]

An additional gap concerns the role of the oligomeric solvents. Even when the chemistry of the surrounding medium is fixed, varying the M_w of the oligomeric solvent can markedly influence the structure and dynamics of soft-nanoparticle dispersions.[19] However, a unified framework that connects concentration-driven deswelling, solvent molecular architecture, and glass fragility is still lacking. In some nominally neutral microgel systems, such concentration-dependent behavior may additionally involve peripheral charged groups and overlapping counterion clouds.

Deswelling has frequently been tuned by varying the solvent quality, temperature, or additives,[13,20] however, a unified diagram that connects concentration-driven deswelling, solvent mass, and glassy fragility remains limited.[21–29] Thus, comparing a good small-molecule solvent with oligomeric solvents of the same polymer chemistry provides a model system: it eliminates changes in chemical functionality while isolating the effect of chain length (or M_w) of solvents on swelling thermodynamics and the local dynamical environment.[19, 30–36]

* Corresponding author, E-mail: lgx@dhu.edu.cn
† These authors contributed equally to this work.
Invited Research Article
Received April 10, 2026; Accepted May 12, 2026; Published online July 10, 2026

In this study, we used soft nanoparticles (SNPs) as a model polymeric colloid.[17] Based on osmotic pressure balance arguments, we first established a concentration-induced deswelling pathway for good small-molecule solvents. We then showed that increasing the solvent mass can also induce deswelling and validated this across all concentrations, forming a unified framework. Small molecular good solvents, such as tricresyl phosphate (TCP), and high molecular mass solvents, such as polystyrene (PS) oligomer/short-chain, are used in experiments and coarse-grained in simulation. Simulations allow convenient evaluation of the diameter and swelling ratio, while experiments can reveal the change in dynamics. The theoretical analysis of deswelling against nanoparticle concentration and solvent molecular mass is based on the osmotic pressure and free energy.

EXPERIMENTAL

Materials

Dodecyltrimethylammonium bromide DTAB (99%), tetrahydrofuran (THF, 99%), styrene (St, 99%), 1,3-diisopropenylbenzene (DIB, 97%), 2,2′-azobis(2-methylpropionitrile) (AIBN, 98%), calcium hydride (CaH2, 99%), isopropanol (IPA, 99%), sec-butyllithium (*s*-BuLi, 97%), cyclohexane (CyH, 98%), tricresyl phosphate (TCP, TCI, 99%), and methanol (MeOH, 98%) were purchased from commercial suppliers and used as received unless otherwise noted. Styrene and DIB were purified by passing them through a column of basic alumina to remove inhibitors prior to use.

Synthesis of SNPs and Linear Polystyrene

The crosslinked polystyrene SNPs were prepared *via* microemulsion polymerization according to previously reported procedures.[37] The particle diameter of the SNPs was controlled by the weight ratio of DTAB to St+DIB. The crosslinking degree, N_c was defined in Ref. [17].

Linear polystyrene (PS) chains with low molecular weights and narrow dispersity were synthesized *via* anionic polymerization. Purified styrene was dissolved in super-dry cyclohexane at a styrene-to-solvent mass ratio of 1:10 with stirring in a glovebox. *sec*-Butyllithium was added dropwise until a persistent orange-yellow color appeared, indicating the formation of living anions. The polymerization was allowed to proceed for 4 h and terminated by the addition of isopropanol. The polymer was precipitated in methanol, collected, and dried under vacuum at 60 °C to constant weight, yield a white powder.

Determination of the Diameters

Microemulsion droplets composed of St and DIB were stabilized by surfactants and subsequently converted into compact SNPs. The latex diameter D_{latex} was measured using dynamic light scattering (DLS) after diluting the crude product 200-fold in water (Fig. S1a in the electronic supplementary information, ESI). The bulk diameter D_{bulk} in the melt state can be estimated using the equation $D_{bulk} \equiv D_{latex} - 2b \approx D_{latex} - 2$ nm, b is the thickness of the surfactant layer. To obtain the swollen particle diameter D_{swo}, dried SNPs powder was redissolved in THF at about 1 mg/mL and measured by DLS using a Malvern Zetasizer with a 532 nm laser source, followed by a 173° detector (Fig. S1b in ESI).

Preparation of SNP Solutions and SNP Oligomer Solutions

PS SNPs and TCP or oligomer solvents were weighed and mixed together at different concentrations. The weight fraction of SNPs was defined as $f_p \equiv m_p/(m_p + m_{sol})$, where m_p is the mass of the SNPs and m_{sol} is the mass of the solvent. Then, a small amount of THF was added to the solution to accelerate dissolution over 5 days. Most of the THF evaporated slowly in the hood. The SNPs solutions were subsequently placed in a vacuum oven at room temperature and 100 °C for 5 days until the weight reached a constant. The SNPs were labeled as D34N60, where D_{bulk} was 34 nm and N_c was 60.

Gel Permeation Chromatography

The molecular weight and dispersity of the linear PS were measured using a Waters ACQUITY APC system, with THF as the eluent. Monodisperse polystyrene standards were used to construct the calibration curve; the resulting GPC curves are shown in Fig. S2 (in ESI).

Linear Viscoelasticity and Glass Transition Temperatures

Small-amplitude oscillatory shear (SAOS) measurements were performed using a stress-controlled rotational rheometer (MARS 60, HAAKE) equipped with 8 mm parallel plates. The angular frequency was varied from 100 rad/s to 0.1 rad/s. Temperature-ramp rheology was conducted on an ARES-G2 rheometer from −50 °C to 180 °C at a heating rate of 5 °C/min and an angular frequency of 10 rad/s (Fig. S3 in ESI). The glass transition temperatures (T_g) were determined from the peak of the phase angle, δ (Fig. S4 in ESI), which reflects the maximum energy dissipation during segmental motion and provides higher sensitivity than calorimetry.[37–41] A nitrogen purge was applied throughout to prevent degradation and moisture absorption.

Simulation of SNPs Swelling in Good Solvents and Oligomers of Varying Molecular Mass

Using a microemulsion polymerization simulation model (details provided in a forthcoming publication), we generated SNPs with a prescribed crosslinking degree (Fig. S5 in ESI). To study their swelling behavior, we performed simulations in the NVT ensemble at a number density $\rho = N/V$ (in units of σ^{-3}) of 0.85 and a temperature T (in units of ε/k_B) of 1.00. Temperature control was achieved using a Nosé-Hoover thermostat with a coupling constant (or damping coefficient) of 0.2. The simulation parameters for both SNPs and solvents followed conventions similar to those used for the coarse-grained (CG) bead-spring polymer model[42]. Non-bonded interactions between CG beads are modeled with a truncated and shifted Lennard-Jones potential, whereas bonded interactions are described by a finite extensible nonlinear elastic (FENE) spring.

In our swelling simulations, the generated SNPs (each containing N_{be} of 766 beads, N_{be} represents the number of beads in each soft cluster) are randomly dispersed in solvents with varying degrees of polymerization N_{sol} (from 2 to 766) or good solvent (N_{sol}=1). The total number of CG beads in the simulation system was 1.915×10^5. The mass fraction of the SNPs, denoted f_p, is defined as the ratio of the SNP mass to the total solution mass. Assuming that the SNPs are dissolved in the solvents and share the same density, the compact volume fraction (dry polymer concentration) v_p (defined later) is

https://doi.org/10.1007/s10118-026-3744-0

equal f_p in the simulation. Because all non-bonded interactions between solvent beads and SNP beads are described by identical parameters, the SNPs swell under good solvent conditions.

$R_g = \sqrt{(1/N_{be})\sum_{i=1}^{N_{be}} |r_i^{SNP} - r_{cm}^{SNP}|^2}$, radius of gyration of SNP. r_i^{SNP} and r_{cm}^{SNP} denote the position of the CG beads constituting the SNPs and center-of-mass positions of the SNPs, respectively. It is denoted as R_g^{bulk} in the melt state and as R_g^v at v_p. The swelling ratio Q in the simulation is defined as $Q \equiv \left(R_g^v/R_g^{bulk}\right)^3$. The swelling process was monitored by tracking the radius of gyration of SNPs as a function of time. Swelling plateaued after 10^4 time units. Therefore, the equilibrium swelling properties were evaluated only after the system had fully equilibrated for at least 10^5 time units. We further defined Q_0, as the swelling ratio in the dilute limit when the solvent polymerization degree $N_{sol}=1$. The effective crosslinking degree, N_c is then estimated from the experimentally established Q_0-N_c relationship (Fig. S6 in ESI).

RESULTS AND DISCUSSION

Concentration-induced Deswelling: Balance of Osmotic Pressure

The swelling state is characterized by the swelling ratio:

$$Q \equiv \left(\frac{R_g^v}{R_g^{bulk}}\right)^3 \equiv \left(\frac{D_v}{D_{bulk}}\right)^3 \equiv \frac{1}{\phi_p} \tag{1}$$

where R_g^{bulk} and R_g^v are described in the simulation section, D_v is the diameter of the swollen SNP in the solution at a certain concentration v_p. Following previous experimental conventions,[17] the compact volume fraction, $v_p \equiv f_p/\left[f_p + (1-f_p)\rho_p/\rho_{sol}\right]$, is the volume fraction of the dry polymer versus the total solution volume, which ranges from 0 to 1. ρ_p is the density of the compact particles and ρ_{sol} is the solvent density.

In the current CG simulation, $v_p \equiv f_p$. The (dry) polymer volume fraction within the swollen microgel is denoted as ϕ_p, which becomes 1 in the bulk state. The effective particle volume fraction $\phi \equiv v_pQ$ was the volume fraction of the microgel divided by the total solution volume. These concentrations are shown in Fig. 1.

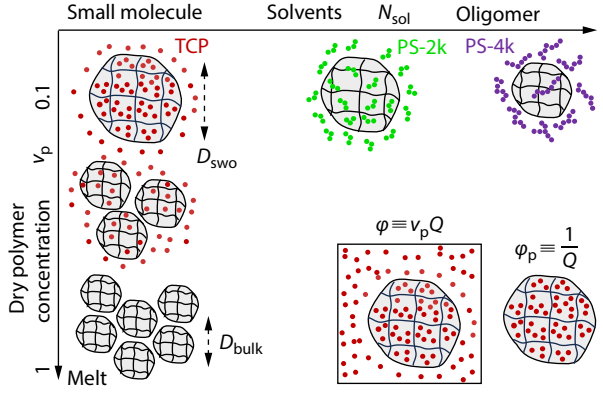

Fig. 1 Schematic illustration of SNP deswelling induced by both dry polymer concentration and solvent molecular mass. The bottom inset figures illustrate the definition of $\phi \equiv v_pQ$ for the swollen-particle volume fraction, and $\phi_p \equiv 1/Q$ for the polymer volume fraction inside one swollen SNP.

Along the *Y*-direction of Fig. 1, increasing the particle concentration intensifies the external osmotic pressure from the surrounding particles, which compresses the microgel. To describe concentration-induced deswelling, we formulated the swelling equilibrium of a nanoparticle as a balance between two competing contributions: the internal osmotic pressure Π_{in} generated within the microgel, and the external osmotic pressure Π_{out} imposed by the surrounding suspension which suppresses swelling at finite particle concentration. Following the standard Flory-Rehner theory,[3,27,43–46] the two contributions of Π_{in} with small molecular good solvents are as follows:

$$\Pi_{mix} = -\frac{k_BT}{l^3}\left[\ln\left(1-\frac{1}{Q}\right)+\frac{1}{Q}+\frac{\chi}{Q^2}\right] \tag{2a}$$

$$\Pi_{el} = \frac{k_BT}{l^3}\frac{1}{N_c}\left(Q^{-\frac{1}{3}}-\frac{1}{2Q}\right) \tag{3}$$

where Π_{mix} represents the osmotic pressure arising from polymer–solvent mixing, Π_{el} is the elastic osmotic pressure resulting from entropic stretching of the polymer network. Here, k_B is the Boltzmann constant, T is the absolute temperature, $l = 1$ is the unit bead length in the simulation. χ is the solvent-polymer interaction parameter, which is determined by fitting. N_c is the average number of monomers between neighboring crosslinks. The external osmotic pressure Π_{out} is imposed by the surrounding solution, which suppresses the swelling at a finite particle concentration. Combining Eqs. 2(a) and (3), the internal osmotic pressure in terms of the swelling ratio Q is

$$\Pi_{in} = \Pi_{mix} - \Pi_{el} = -k_BT\left[\ln\left(1-\frac{1}{Q}\right)+\frac{1}{Q}+\frac{\chi}{Q^2}+\frac{1}{N_c}\left(Q^{-\frac{1}{3}}-\frac{1}{2Q}\right)\right] \tag{4}$$

Increasing the particle concentration within the bath led to the development of significant external osmotic pressure. While a previous study[43] used empirical equations such as that of Speedy[47], we found that the Carnahan and Starling formulation[48] provides a more robust theoretical basis for describing this pressure in our specific soft colloidal system.[49–51] This external contribution is then represented by: $\Pi_{out}(\phi) = \rho_n k_BT(1+\phi+\phi^2-\phi^3)/(1-\phi)^3$. The number density, ρ_n is v_p/N_{be}. As revealed in the subsequent fitting, one adjustable parameter S is needed to rescale the magnitude of the osmotic compression.[52] Substituting ρ_n and ϕ into Π_{out} yields:

$$\Pi_{out}(v_p, Q) = k_BT\frac{Sv_p}{N_{be}}\cdot\frac{1+v_pQ+(v_pQ)^2-(v_pQ)^3}{(1-v_pQ)^3} \tag{5a}$$

The equilibrium swelling state is then determined by the osmotic pressure condition $\Pi_{in} = \Pi_{mix} - \Pi_{el} = \Pi_{out}(v_p, Q)$, resulting in:

$$\left[\ln\left(1-\frac{1}{Q}\right)+\frac{1}{Q}+\frac{\chi}{Q^2}+\frac{1}{N_c}\left(Q^{-\frac{1}{3}}-\frac{1}{2Q}\right)\right]+\frac{Sv_p}{N_{be}}\cdot\frac{1+v_pQ+(v_pQ)^2-(v_pQ)^3}{(1-v_pQ)^3}=0 \tag{6a}$$

Eq. 6(a) therefore describes concentration-induced deswelling as the result of a balance between the particle's inter-

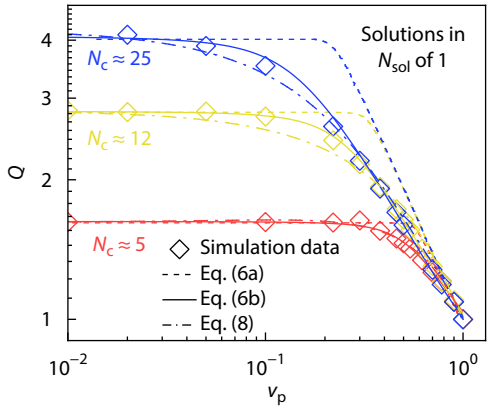

Fig. 2 Swelling ratio Q denotes the concentration-dependent swelling ratio, in good solvent of N_{sol} = 1. Q is also dependent on the crosslinking degrees (N_c) of microgels. Open diamond symbols are results calculated from CG molecular dynamics simulations. Dashed curves show the fitting of the original Eq. (6a). Solid curves are fitted to the modified Eq. (6b). χ and S are fitting variables. Dash-dotted curves denote an empirical explicit Eq. (8).

nal swelling pressure and the concentration-dependent osmotic compression exerted by neighboring particles. Q was obtained from the CG simulation and is plotted in Fig. 2. Although Eq. (6) captures the overall trend of concentration-induced deswelling, as indicated by the dashed curve in Fig. 2; it does not reproduce the simulation data over intermediate concentration ranges.

To account for the deviation, we realize that ϕ in the Carnahan–Starling formulation should only range from 0 to the close packing of the hard sphere. However, in our soft colloids, v_pQ ranged from 0 to 1. To map v_pQ also from 0 to close packing and inspired by the formulation of Speedy, we reshape this term in Π_{out} as $v_pQ\phi_{max}$, and ϕ_{max} is chosen as 0.742.[53] We also found that the $\phi + \phi^2 - \phi^3$ part is not crucial; thus, Π_{out} is modified as Eq. (5b), and we obtained the governing Eq. (6b).

$$\Pi_{out}(v_p, Q) \approx k_BT\frac{Sv_p}{N_{be}}\cdot\frac{1}{(1-\phi)^3} = k_BT\frac{Sv_p}{N_{be}}\cdot\frac{1}{(1-v_pQ\phi_{max})^3} \quad (5b)$$

$$\left[\ln\left(1-\frac{1}{Q}\right)+\frac{1}{Q}+\frac{\chi}{Q^2}+\frac{1}{N_c}\left(Q^{-\frac{1}{3}}-\frac{1}{2Q}\right)\right]+\frac{Sv_p}{N_{be}}\cdot\frac{1}{(1-v_pQ\phi_{max})^3}=0 \quad (6b)$$

Eq. 6(b), with only two fitting parameters, χ and S, fits well with the simulation results shown in Fig. 2. χ and S depended on N_c (Fig. S7 in ESI, for N_c=5, 12 and 25, χ is 0.58, 0.31, 0.25, respectively, while S is 13.74, 16.61, 25.87, respectively).

Deswelling Induced by Oligomeric Solvents

As shown in the X-direction of Fig. 1, longer solvent molecules have a lower mixing entropy, which suppresses their penetration into the network and drives deswelling. When a microgel is placed in a solvent containing oligomers, the mixing term changes from Eq. (2a) to Eq. (2b), where N_{sol} is the number of beads in oligomeric solvents. The elastic part remains the same as that in Eq. (3). Therefore, a unified description of the deswelling is shown in Eq. (6c). The simulation results are shown in Fig. 3, along with the curve of Eq. (6c), fitted by the sets of χ and S (Fig. S8 in ESI). N_{sol} varied from 1, 2 to 766. The implicit Eq. (6c) captures the swelling ratio Q at arbitrary particle concentration v_p and solvent mass N_{sol}. Therefore, the deswelling behavior in oligomeric solvents can be interpreted as a coupled consequence of solvent-mass-induced solvent exclusion and concentration-induced crowding. When the particle concentration increases, deswelling releases solvent molecules, creating excess space that enables more efficient packing by lowering the effective particle volume fraction, which would also be entropy-driven.

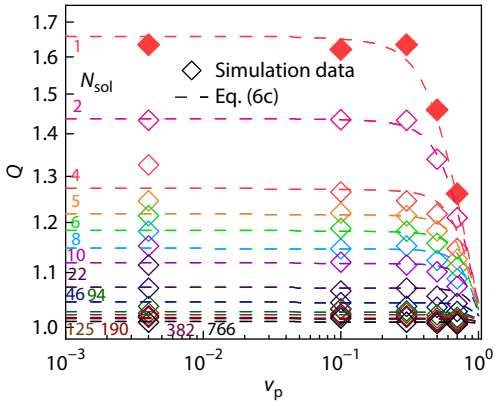

Fig. 3 Coupled effects of solvent molecular mass and particle volume fraction on the deswelling behavior of nanoparticles at N_c = 5. Filled (N_{sol}=1) and open (N_{sol}>1) diamonds denote the simulation data. Dashed curves represent fits to Eq. (6c) by χ and S.

$$\Pi_{mix}(Q) = -k_BT\left\{\frac{1}{N_{sol}}\left[\frac{1}{Q}+\ln\left(1-\frac{1}{Q}\right)\right]+\frac{\chi}{Q^2}\right\} \quad (2b)$$

$$\frac{1}{N_{sol}}\left[\ln\left(1-\frac{1}{Q}\right)+\frac{1}{Q}\right]+\frac{\chi}{Q^2}+\frac{1}{N_c}\left(Q^{-\frac{1}{3}}-\frac{1}{2Q}\right)+\frac{Sv_p}{N_{be}}\cdot\frac{1}{(1-v_pQ\phi_{max})^3}=0 \quad (6c)$$

At v_p = 0.004 and 0.1, the simulated data in Fig. 3 can be replotted, as shown in Fig. 4, to show the situation at the dilution limit. As the N_{sol} of the solvent increases, it becomes more difficult for these longer chains to penetrate the micro-

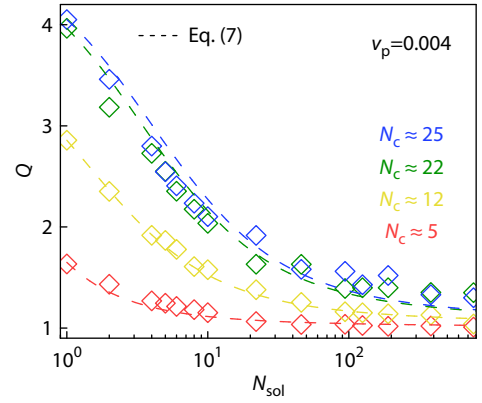

Fig. 4 Swelling ratio Q (extracted from Fig. 3 at the dilute limit of v_p) replotted against N_{sol} for microgel at N_c of 5, 12, 22, 25. Open diamonds are simulation data. Solid line, is smoothed curve from fitted results by Eq. (6c) at v_p of 0.004. Different color dashed curves are fitted by explicit Eq. (7).

https://doi.org/10.1007/s10118-026-3744-0

gel, leading to a reduction in the swelling ratio. The swelling ratio of the nanoparticles decreased with an increase N_{sol}. Both χ and S changed with N_{sol} in Fig. 4. For a straightforward quantitative description of the deswelling behavior, we evaluated more simulation data and explicit equations in the following section.

Explicit Empirical Relationships

In addition to the microgel at N_c in the dilute solutions of various N_{sol} (appearing in Fig. 3 at v_p=0.004), we also simulated the microgels of other N_c. Inspired by Eq. (6c), rescaling of $(N_{sol}-1)/N_c$ was proposed. $[Q(N_{sol})-1]/[Q_0(N_{sol}=1)-1]$ could normalize the Y-axis such that when X went to 0, Y was 1, and when X went to 1, Y was 0. The simulated data are plotted in Fig. 4 and normalized in Fig. S9(a) (in ESI) revealing a universal pattern. We propose an explicit form of Eq. (7), where k was fitted as 4.5 (dashed curves). This relation captures the deswelling against N_{sol} under dilute conditions for microgels of arbitrary N_c, and will be used for the analysis in Section "**Relaxation Time and Fragility Tuned by Deswelling in Oligomeric Solvent**".

The trend in Fig. 2 has three features: first, at small v_p, Q is constant at Q_0; second, at v_p=1, Q should be fixed at 1 as melts; third, the derivative Q' should be 1 (because v_p is proportional to the number density and inversely proportional to the particle volume). To satisfy all three conditions, we propose explicit Eq. (8). As shown in Fig. 2, an excellent agreement with the simulation data was obtained using the fitted parameters Q_0=1.61, 2.82,4.21 and m=3.53, 1.99, and 3.88, respectively. We also replotted Fig. 2 by using the same normalized Q_0 in Fig. S9(b) (in ESI).

$$\frac{Q(N_{sol})-1}{Q_0-1}=\frac{1}{1+k\lg\left(1+\frac{N_{sol}-1}{N_c}\right)} \tag{7}$$

$$Q(v_p)=2-v_p+(Q_0-2)(1-v_p)^m \tag{8}$$

$$\frac{Q(v_p,N_{sol})-1}{Q_0-1}=\frac{1}{1+k\lg\left(1+\frac{N_{sol}-1}{N_c}\right)} \tag{9}$$

Combining Eqs. (7) and (8) against the solvent mass and particle volume fraction, we have a comprehensive explicit Eq. (9), which captures the general swelling behavior under any condition. This equation integrates the effects of the solvent mass and particle volume fractions, providing a simple yet quantitative description of the deswelling of microgels.

Linear Viscoelasticity of SNPs in Oligomeric Solvent

D34N60 (SNPs) were dispersed in a small molecular solvent (TCP) and different oligomer matrices. The oligomeric solvents were PS with M_w of 1870, 3150, and 4650 g/mol and PDI values of 1.02, 1.06, and 1.08, respectively (Table S1 and Fig. S2 in ESI). The resulting solutions exhibited a good distribution of the D34N60 SNPs because the chemistry of the nanoparticles was the same as that of the solvent. The linear viscoelasticity of the SNPs in different solvents M_w was characterized using SAOS. The experimental details of the preparation and characterization of PS nanocomposites are included in the Methods section. The master curves of SNPs were created using time-temperature superposition (TTS) with horizontal and vertical shifting at the reference temperature $T_{ref}=T_g$+10 °C, resulting in the corresponding shifting factor a_T. The corresponding WLF equation is shown in Fig. S11 (in ESI). This ensured the comparison at an equal time scale for the Kuhn segment.

When the SNPs were added to TCP, the storage and loss moduli (G' and G'', filled and open squares, respectively) clearly depended on the concentration (Fig. 5a). When v_p was 0.20 or lower, the solution was viscous dominant. At v_p = 0.38 or higher, an elastic plateau emerges owing to the particle caging. The terminal relaxation time τ_{iso} was obtained at the crossover of the extrapolated $G' \sim \omega^2$ and $G'' \sim \omega^1$, as shown in Fig. 5(a). Fig. 5(b) shows G' and G'' (filled and open circles, respectively) for SNP oligomer solutions over a broad frequency range at a constant v_p of 0.54, but with different solvent M_w. On intermediate timescales, G' exhibits a rubber plateau, and after the plateau, the crossover frequencies are identified as the characteristic time scales: the terminal relaxation time of the SNP oligomer solutions. The plateau became narrower with a higher solvent M_w.

Relaxation Time and Fragility Tuned by Deswelling in Oligomeric Solvent

The relaxation time of the SNP oligomer solutions was plotted

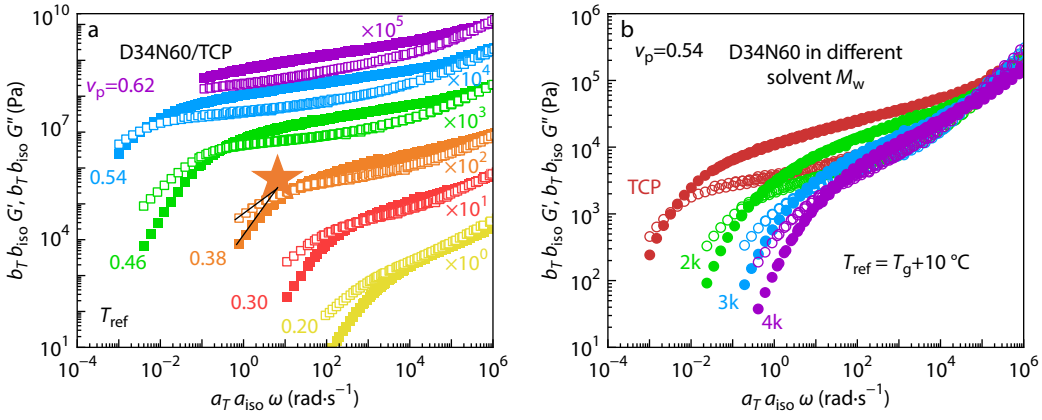

Fig. 5 Storage modulus G' and loss modulus G'' as a function of angular frequency ω at temperatures $T_{ref}=T_g$+10 °C for various samples. (a) D34N60 in TCP at different volume fractions v_p. The different colors correspond to varying volume fractions v_p, ranging from 0.20 to 0.62. (b) D34N60 in different solvent M_w (oligo-PS of 2k, 3k, 4k g/mol) at constant v_p of 0.54.

https://doi.org/10.1007/s10118-026-3744-0

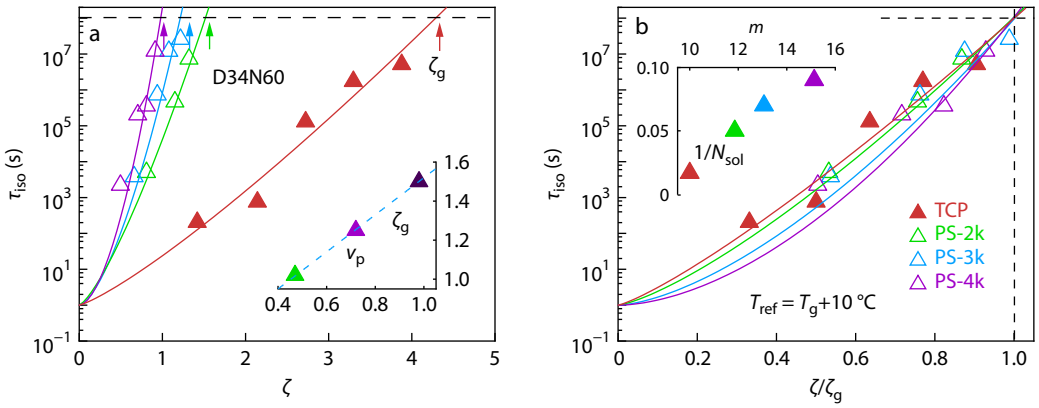

Fig. 6 Relaxation time versus extrapolated volume fraction. (a) The relaxation time τ_{iso} of SNP-oligomer solutions is plotted against the extrapolated volume fraction ζ. Solid curves are fitted using Eq. (10).τ_{iso} for solutions with larger solvent M_w increases exponentially, resembling more fragile molecular glasses. For smaller solvent M_w, the increase in τ_{iso} is less pronounced, indicating more robust dynamics. (b) The relaxation time (τ_{iso}) is replotted against the normalized volume fraction (ζ/ζ_g), where ζ_g is determined by $\tau_{iso}|_{\zeta_g} \equiv 10^8$ s for each different oligomer chain. The inset in (b) shows the fragility index m, which increases with the elasticity of the deswellen SNPs, further confirming the transition from a strong glass to a fragile glass as solvent mass increase.

against the extrapolated volume fraction $\zeta \equiv v_p \cdot Q_0$, which is more suitable for soft colloids[43]. For solutions with higher solvent M_w, the relaxation time τ_{iso} increases exponentially, resembling the behavior of more fragile molecular glasses (Fig. 6a). In contrast, for a smaller solvent M_w, the increase in τ_{iso} was less pronounced, showing stronger glass dynamics.

At $T_g + 10$ °C, we can compare the slow dynamics on an equal basis (Fig. 6a). Building on our previous investigations in the solution state[17], we apply Eq. (10) to fit the τ_{iso} of the D34N60 solutions. The prefactor time scale τ_0 is fixed as 0.1 s, and it contains two fitting parameters (α and β).

$$\tau_{iso} = \tau_0 \exp\left[(\beta \cdot \zeta)^{\alpha}\right] \quad (10)$$

Using the extrapolated volume fraction, we defined the glassy state of the solution as the point at which the isochronal relaxation time satisfied $\tau_{iso}|_{\zeta_g} \equiv 10^8$s. This definition allows us to replicate Fig. 6(a) in terms of the normalized volume fraction ζ/ζ_g , yielding Fig. 6(b), which serves as an Angell plot. The fragility index is defined as $m \equiv \mathrm{d}\left(\lg\tau_{iso}\right)/\mathrm{d}\left(\zeta/\zeta_g\right)\big|_{\zeta=\zeta_g}$. The resulting m is insensitive to the numerical choice of $\tau_{iso}|_{\zeta_g}$ and ζ_g. Fig. S10(a) (in ESI) shows the fragility index m, which quantifies the sensitivity of τ_{iso} to the changes in ζ/ζ_g. Clearly, m increases with the solvent M_w, indicating that longer polymer chains induce a more fragile glass transition behavior. This analysis highlights how the solvent M_w can be used to tune the dynamics of SNP oligomer solutions, with larger chains leading to a more fragile glass state.

The master curve of Fig. S9(a) (in ESI) was used to predict the swelling ratio Q_0(under dilute conditions) of D34N60 in solvents with different N_{sol} (Fig. S10a in ESI). The predicted values suggest that D34N60 deswells from Q_0=7.26 in THF to 3.87, 3.14 and 2.71 in 2k, 3k, and 4k solvents, respectively (N_{sol} of 1, 17.8, 30, and 44.3). The contour length of TCP was approximately 2 (its N_{sol}). We experimentally measured the Q_0 of D34N60 in TCP as 6.98. This point overlaps well in Figs. S9(a) and S10(a) (in ESI), further validating master Eq. (7). Given these Q_0, we can use the Q_0-N_c relationship (Fig. S6 in ESI) to estimate their effective $N_{c,sol}$, which inversely represents the elasticity of the swollen SNPs in the solvents of N_{sol}. The inset in Fig. 6(b) shows a strong correlation with the observed fragility. Because they are the same as those of D34N60, this is also proportional to the elastic energy. The analysis used in Fig. 5 of a previous work[17] is also compared in Fig. S10(b) (in ESI), further confirming that fragility is governed by the elasticity and elastic energy of the particles.

CONCLUSIONS

We systematically varied the nanoparticle concentration and the solvent molecular mass. Deswelling functions were derived from a free-energy analysis and validated against simulation results, and empirical expressions were constructed explicitly. In a good solvent, increasing SNP concentration drives deswelling through crowding, leading to a progressively more compact particle state. Replacing the solvent with short-chain oligomers provides a distinct route for reducing the swelling ratio at low particle concentrations. By tuning the molecular weight of the solvent oligomer, one can modulate solvent penetration and uptake by SNPs, enabling deswelling even under weakly crowded conditions. Importantly, increasing the solvent mass also qualitatively alters the glassy dynamics, promoting a transition from strong to fragile behavior, as observed in the experiments. Enhanced deswelling makes SNPs more difficult to detect. These results establish solvent mass and particle concentration as two linked control parameters connecting equilibrium swelling (softness) to vitrification and fragility of soft colloids.

Conflict of Interests

The authors declare no interest conflict.

Electronic Supplementary Information

Electronic supplementary information (ESI) is available free of

https://doi.org/10.1007/s10118-026-3744-0

charge in the online version of this article at http://doi.org/10.1007/s10118-026-3744-0.

Data Availability Statement

The data supporting the findings of this study are available from the corresponding author upon reasonable request.

ACKNOWLEDGMENTS

This work was financially supported by the National Natural Science Foundation of China (Nos. 22403105 and 22473025), the China Postdoctoral Science Foundation (No. 2025M771120), and the Shanghai Municipal Education Commission.

REFERENCES

1 Rubinstein, M.; Colby, R. H. *Polymer physics*; Oxford university press, **2003**, p. 137–196.
2 Likos, C. N. Effective interactions in soft condensed matter physics. *Phys. Rep.* **2001**, *348*, 267–439.
3 Flory, P. J.; Rehner, J. Statistical mechanics of cross-linked polymer networks ii. Swelling. *J. Chem. Phys.* **1943**, *11*, 521–526.
4 Huggins, M. L. Solutions of long chain compounds. *J. Chem. Phys.* **1941**, *9*, 440–440.
5 Flory, P. J. Thermodynamics of high polymer solutions. *J. Chem. Phys.* **1942**, *10*, 51–61.
6 Berthier, L.; Biroli, G. Theoretical perspective on the glass transition and amorphous materials. *Rev. Mod. Phys.* **2011**, *83*, 587–645.
7 Ediger, M. D.; Angell, C. A.; Nagel, S. R. Supercooled liquids and glasses. *J. Phys. Chem.* **1996**, *100*, 13200–13212.
8 Angell, C. A. Relaxation in liquids, polymers and plastic crystals — strong/fragile patterns and problems. *J. Non-Cryst. Solids* **1991**, *131-133*, 13-31.
9 Debenedetti, P. G.; Stillinger, F. H. Supercooled liquids and the glass transition. *Nature* **2001**, *410*, 259–267.
10 Adam, G.; Gibbs, J. H. On the temperature dependence of cooperative relaxation properties in glass-forming liquids. *J. Chem. Phys.* **1965**, *43*, 139–146.
11 Lopez, C. G.; Lohmeier, T.; Wong, J. E.; Richtering, W. Electrostatic expansion of polyelectrolyte microgels: Effect of solvent quality and added salt. *J. Colloid Interface Sci.* **2020**, *558*, 200–210.
12 Karg, M.; Pich, A.; Hellweg, T.; Hoare, T.; Lyon, L. A.; Crassous, J. J.; Suzuki, D.; Gumerov, R. A.; Schneider, S.; Potemkin, I. I.; et al. Nanogels and microgels: From model colloids to applications, recent developments, and future trends. *Langmuir* **2019**, *35*, 6231–6255.
13 Plamper, F. A.; Richtering, W. Functional microgels and microgel systems. *Acc. Chem. Res.* **2017**, *50*, 131–140.
14 Pellet, C.; Cloitre, M. The glass and jamming transitions of soft polyelectrolyte microgel suspensions. *Soft Matter* **2016**, *12*, 3710–3720.
15 Conley, G. M.; Aebischer, P.; Nöjd, S.; Schurtenberger, P.; Scheffold, F. Jamming and overpacking fuzzy microgels: deformation, interpenetration, and compression. *Sci. Adv.* **2017**, *3*, e1700969.
16 Del Monte, G.; Zaccarelli, E. Numerical study of neutral and charged microgel suspensions: from single-particle to collective behavior. *Phys. Rev. X* **2024**, *14*, 041067.
17 Zhu, Y.; Gao, Y.; Gao, J.; Zhang, R.; Liu, G. Quantifying the fragility–elasticity relationship in uncharged ultrasmall polymeric colloids. *ACS Macro Letters* **2026**, *15*, 137–142.
18 Marín-Aguilar, S.; Zaccarelli, E. Unexpected behavior of ultra-low-crosslinked microgels in crowded conditions. *Proc. Natl. Acad. Sci.* **2026**, *123*, e2530546123.
19 Ouyang, X.; Luo, J.; Li, T.; Zhu, Y.; Yu, W.; He, J.; Zhang, P.; Liu, G. The second network of soft-nanoparticles in linear polymers of the same chemistry. *Polymer* **2023**, *283*, 126216.
20 Lyon, L. A.; Fernandez-Nieves, A. The polymer/colloid duality of microgel suspensions. *Annu. Rev. Phys. Chem.* **2012**, *63*, 25–43.
21 Gerelli, Y.; Camerin, F.; Bochenek, S.; Schmidt, M. M.; Maestro, A.; Richtering, W.; Zaccarelli, E.; Scotti, A. Softness matters: effects of

Graphical Abstract

Microgels Deswell against Concentration and Solvent Molecular Mass

Yi-Hui Zhu, Qing-Zhi Zou, Zhan-Hui Gan, Yi-Fu Ruan, Kai Qi, Peng-Fei Zhang, and Geng-Xin Liu

Donghua University; Shanghai Institute of Microsystem and Information Technology, Chinese Academy of Sciences; University of Chinese Academy of Sciences; South China University of Technology

Microgel deswelling is controlled by two coupled factors: the nanoparticle concentration and solvent molecular mass. A higher nanoparticle concentration strengthens osmotic compression, whereas a larger solvent molecular mass reduces network penetration, thereby promoting a transition from swollen to compact particle bulk states, leading to a more fragile soft colloidal glass.

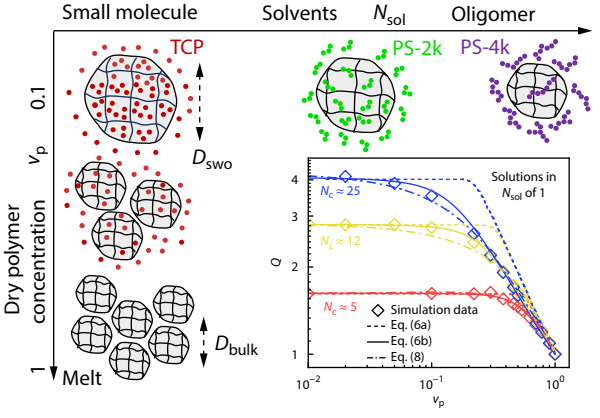

Chinese J. Polym. Sci., 2026 *https://doi.org/10.1007/s10118-026-3744-0*

compression on the behavior of adsorbed microgels at interfaces. *Soft Matter* **2024**, *20*, 3653–3665.
22 Pelaez-Fernandez, M.; Souslov, A.; Lyon, L. A.; Goldbart, P. M.; Fernandez-Nieves, A. Impact of single-particle compressibility on the fluid-solid phase transition for ionic microgel suspensions. *Phys. Rev. Lett.* **2015**, *114*, 098303.
23 Scotti, A.; Pelaez-Fernandez, M.; Gasser, U.; Fernandez-Nieves, A. Osmotic pressure of suspensions comprised of charged microgels. *Phys. Rev. E* **2021**, *103*, 012609.
24 Camerin, F.; Gnan, N.; Ruiz-Franco, J.; Ninarello, A.; Rovigatti, L.; Zaccarelli, E. Microgels at interfaces behave as 2d elastic particles featuring reentrant dynamics. *Phys. Rev. X* **2020**, *10*, 031012.
25 Urich, M.; Denton, A. R. Swelling, structure, and phase stability of compressible microgels. *Soft Matter* **2016**, *12*, 9086–9094.
26 Bouhid de Aguiar, I.; van de Laar, T.; Meireles, M.; Bouchoux, A.; Sprakel, J.; Schroën, K. Deswelling and deformation of microgels in concentrated packings. *Sci. Rep.* **2017**, *7*, 1–11.
27 Mattsson, J.; Wyss, H. M.; Fernandez-Nieves, A.; Miyazaki, K.; Hu, Z.; Reichman, D. R.; Weitz, D. A. Soft colloids make strong glasses. *Nature* **2009**, *462*, 83–86.
28 Larin, D. E.; Shibaev, A. V.; Liu, C. Y.; Emelyanenko, A. V. The effect of dynamic cross-links and mesogenic groups on the swelling and collapse of polymer gels. *Giant* **2024**, *20*, 100341.
29 Hwang, J.; Martinez, D. V.; Martinez, E. J.; Metavarayuth, G.; Goodlett, D.; Wang, Q.; Ganewatta, M.; Kent, M. S.; Tang, C. Highly swellable hydrogels prepared from extensively oxidized lignin. *Giant* **2022**, *10*, 100106.
30 Tuteja, A.; Duxbury, P. M.; Mackay, M. E. Polymer chain swelling induced by dispersed nanoparticles. *Phys. Rev. Lett.* **2008**, *100*, 077801.
31 Maiz, J.; Verde-Sesto, E.; Asenjo-Sanz, I.; Mangin-Thro, L.; Frick, B.; Pomposo, J. A.; Arbe, A.; Colmenero, J. Disentangling component dynamics in an all-polymer nanocomposite based on single-chain nanoparticles by quasielastic neutron scattering. *Macromolecules* **2022**, *55*, 2320–2332.
32 Xu, B.; Xu, H.; Song, Y.; Zheng, Q. Segmental dynamics and linear rheology of nearly athermal all-polystyrene nanocomposites. *Compos. Sci. Technol.* **2019**, *177*, 111–117.
33 Tuteja, A.; Mackay, M. E.; Hawker, C. J.; Van Horn, B.; Ho, D. L. Molecular architecture and rheological characterization of novel intramolecularly crosslinked polystyrene nanoparticles. *J. Polym. Sci., Part B: Polym. Phys.* **2006**, *44*, 1930–1947.
34 Mackay, M. E.; Dao, T. T.; Tuteja, A.; Ho, D. L.; Van Horn, B.; Kim, H.-C.; Hawker, C. J. Nanoscale effects leading to non-einstein-like decrease in viscosity. *Nat. Mater.* **2003**, *2*, 762–766.
35 Chen, T.; Zhao, H. Y.; Shi, R.; Lin, W. F.; Jia, X. M.; Qian, H. J.; Lu, Z. Y.; Zhang, X. X.; Li, Y. K.; Sun, Z. Y. An unexpected n-dependence in the viscosity reduction in all-polymer nanocomposite. *Nat. Commun.* **2019**, *10*, 1–8.
36 Cui, T.; Zhu, Y.; Liu, S.; Huang, Q. Extensional rheology of all-polystyrene nanocomposites. *Phys. Fluids* **2024**, *36*, 113120.
37 Luo, J.; Zhu, Y.; Ruan, Y.; Wu, W.; Ouyang, X.; Du, Z.; Liu, G. Diameter and elasticity governing the relaxation of soft-nanoparticle melts. *Macromolecules* **2021**, *54*, 8077–8087.
38 Rieger, J. The glass transition temperature tg of polymers—comparison of the values from differential thermal analysis (DTA, DSC) and dynamic mechanical measurements (torsion pendulum). *Polym. Test.* **2001**, *20*, 199–204.
39 Hagen, R.; Salmén, L.; Lavebratt, H.; Stenberg, B. Comparison of dynamic mechanical measurements and tg determinations with two different instruments. *Polym. Test.* **1994**, *13*, 113–128.
40 Gracia-Fernández, C. A.; Gómez-Barreiro, S.; López-Beceiro, J.; Tarrío Saavedra, J.; Naya, S.; Artiaga, R. Comparative study of the dynamic glass transition temperature by DMA and TMDSC. *Polym. Test.* **2010**, *29*, 1002–1006.
41 Napolitano, S.; Glynos, E.; Tito, N. B. Glass transition of polymers in bulk, confined geometries, and near interfaces. *Rep. Prog. Phys.* **2017**, *80*, 036602.
42 Zou, Q.; Zhu, Y.; Ruan, Y.; Zhang, R.; Liu, G. Coarse-grained soft-clusters remain non-diffusing in the melt state. *Giant* **2021**, *8*, 100070.
43 van der Scheer, P.; van de Laar, T.; van der Gucht, J.; Vlassopoulos, D.; Sprakel, J. Fragility and strength in nanoparticle glasses. *ACS Nano* **2017**, *11*, 6755–6763.
44 Voudouris, P.; Florea, D.; van der Schoot, P.; Wyss, H. M. Micromechanics of temperature sensitive microgels: Dip in the poisson ratio near the lcst. *Soft Matter* **2013**, *9*, 7158.
45 Hashmi, S. M.; Dufresne, E. R. Mechanical properties of individual microgel particles through the deswelling transition. *Soft Matter* **2009**, *5*, 3682.
46 Lopez, C. G.; Richtering, W. Does flory–rehner theory quantitatively describe the swelling of thermoresponsive microgels. *Soft Matter* **2017**, *13*, 8271–8280.
47 Speedy, R. J. The equation of state for the hard sphere fluid at high density. The glass transition. *Physica B+C* **1983**, *121*, 153–161.
48 Carnahan, N. F.; Starling, K. E. Equation of state for nonattracting rigid spheres. *J. Chem. Phys.* **1969**, *51*, 635–636.
49 Pyett, S.; Richtering, W. Structures and dynamics of thermosensitive microgel suspensions studied with three-dimensional cross-correlated light scattering. *J. Chem. Phys.* **2005**, *122*, 034709.
50 Stieger, M.; Pedersen, J. S.; Lindner, P.; Richtering, W. Are thermoresponsive microgels model systems for concentrated colloidal suspensions? A rheology and small-angle neutron scattering study. *Langmuir* **2004**, *20*, 7283–7292.
51 Carrier, V.; Petekidis, G. Nonlinear rheology of colloidal glasses of soft thermosensitive microgel particles. *J. Rheol.* **2009**, *53*, 245–273.
52 Wilcox, K. G.; Kozawa, S. K.; Morozova, S. Fundamentals and mechanics of polyelectrolyte gels: Thermodynamics, swelling, scattering, and elasticity. *Chem. Phys. Rev.* **2021**, *2*, 041309.
53 Richbourg, N. R.; Peppas, N. A. The swollen polymer network hypothesis: Quantitative models of hydrogel swelling, stiffness, and solute transport. *Prog. Polym. Sci.* **2020**, *105*, 101243.